frontiers | Frontiers in Environmental Science

ORIGINAL RESEARCH
published: 13 May 2022
doi: 10.3389/fenvs.2022.893180

Extreme Hydrological Events and Reservoir Methane Emissions

Bradford S. Sherman[1,2]* *and Phillip W. Ford*[3]

[1]CSIRO Land and Water, Canberra, ACT, Australia, [2]Reservoir Doctors Pty Ltd., Duffy, ACT, Australia, [3]CSIRO Oceans and Atmosphere, Canberra, ACT, Australia

Floating chamber measurements of CH_4 emissions from Cotter Reservoir (Canberra, Australia) were performed on five occasions between October 2010 and April 2012. The timing of the measurements spanned the first major flood events that followed drought-breaking rains that ended the Millenium Drought in southeast Australia. The flood events were the largest in 26 years and followed the 3 lowest flow years on record. The floods warmed the hypolimnion of this normally monomictic reservoir by ~8°C during the first summer and by ~3°C during the second summer of the study compared to "normal" summer hypolimnion temperatures. In addition, the floods carried large amounts of vegetation and soil that had accumulated in the catchment during previous years. Average CH_4 emissions prior to the flooding were low (4.3 mg-CH_4 m^{-2} d^{-1}) and relatively uniform across 8 measurement sites spaced along the long axis of the reservoir. Following the first floods, which occurred during spring and summer 2010–2011, the mean reservoir CH_4 emission increased to 99 mg-CH_4 m^{-2} d^{-1} with emissions at the upstream end of the reservoir approximately 100 times greater than emissions near the dam wall. The following year (2011–2012) average emissions were lower (30 mg-CH_4 m^{-2} d^{-1}) and the longitudinal gradient weakened. A major flood occurred in autumn 2012 and warmed the hypolimnion by ~3 C, but emissions did not change much in response. We hypothesize that the changes in mean reservoir CH_4 emission can be attributed to both thermal enhancement of sediment methanogenesis by a factor of 2–7, and to the supply of fresh organic matter from the catchment by a factor of 3.

Keywords: methane-CH_4, reservoir, hydrology, flood, climate change, spatiotemporal variability

OPEN ACCESS

Edited by:
Daniel F. McGinnis,
Université de Genève, Switzerland

Reviewed by:
Ryan P. McClure,
Virginia Tech, United States
Luana S. Basso,
National Institute of Space Research (INPE), Brazil

***Correspondence:**
Bradford S. Sherman
BradfordS.Sherman@icloud.com

Specialty section:
This article was submitted to Biogeochemical Dynamics, a section of the journal Frontiers in Environmental Science

Received: *10 March 2022*
Accepted: *21 April 2022*
Published: *13 May 2022*

Citation:
Sherman BS and Ford PW (2022) Extreme Hydrological Events and Reservoir Methane Emissions. Front. Environ. Sci. 10:893180. doi: 10.3389/fenvs.2022.893180

1 INTRODUCTION

Methane in the atmosphere is a strong absorber of infra-red (7.6 μm) radiation and is the second most radiatively active atmospheric gas after CO_2. Increases in CH_4 concentration in the atmosphere affect the Earth's radiation balance and contribute to global warming. The global average atmospheric concentration of methane has increased from approximately 700 ppb at the start of the industrial era to 1880 ppb in 2020. The trajectory of concentration was not one of unbroken rise, with a 7-year plateau from 2000 to 2007. Most of the increase has been attributed to human activities particularly to leakage from oil, coal, and natural gas extraction, rice paddies, reservoirs, land fills, and emissions from farmed ruminants. These anthropogenic emissions are added to the pre-existing natural emissions from lakes (albeit now often perturbed from pristine conditions by human modified nutrient inputs), wetlands, and geologic emissions (Etiope and Schwietzke, 2019). The

global methane emissions are predominantly balanced by an atmospheric sink term due to reaction with OH radical in the troposphere with a methane lifetime of 9.1 years (Prather et al., 2012), and controlled largely by the concentration of OH.

The post 2007 increase in the atmospheric CH_4 inventory has been attributed to changes in the strength of both the natural and anthropogenic components as well as changes in the tropospheric oxidation rate, but these attributions remain uncertain and in some cases contradictory (Turner et al., 2019; Lan et al., 2021). There are only limited, globally available, parameters (CH_4 concentration, $\delta C^{13}CH_4$, and δD^2CH_4) available to deconvolve the global (or twin hemisphere) concentration signal, while several sources share common isotopic characteristics. The alternative bottom-up approach to source identification suffers from an inability to enumerate all the sources in each category of emitter, as well as a lack of precision in quantifying the individual emissions, or to model them accurately. Consequently, there is a mismatch between the two approaches which has not been resolved yet, as well as substantial uncertainties in estimating the size of the various sources.

Irrespective of the sources of the CH_4, consideration of the global warming equivalents (Lynch et al., 2020) shows that for times shorter than 100 years, CH_4 mitigation strategies can produce reductions in global warming faster than equi-molar CO_2 reductions due to the much longer residence time of CO_2 vis a vis the lifetime of CH_4 (Shindell et al., 2012; Turner et al., 2019; Lynch et al., 2020). The benefits of prompt CH_4 mitigation (i.e., well before 2050) have now been recognized in the policy sphere and adopted recently as an international priority measure at COP 26 (albeit with some nations abstaining).

Reduction in methane emission from reservoirs have emerged now as a potentially promising mitigation opportunity. Reservoirs as well as ponds and lakes are now included in the global GHG accounting protocols, and quantified reductions are recognized as contributions to agreed national commitments. Furthermore, since reservoirs are engineered structures, there is potential scope to implement changes in their operating rules designed to lower CH_4 emissions. Aesthetic, environmental conservation, and biodiversity considerations may limit similar manipulations for natural lakes and ponds. In addition, the mitigation methods appropriate for reservoirs may not carry over to lakes, given the different drivers controlling CH_4 emissions in the two types of systems (Deemer and Holgerson, 2021).

In light of the evidence (discussed further below) that increased catchment loads, implicitly containing terrestrial organic carbon, lead to increased CH_4 emissions, catchment manipulation to limit carbon-rich sediment inputs is another potential mitigation mechanism. The obstacle to implementation of mitigation measures in either the catchment, or the reservoir itself, is the lack of the underpinning and integrated mechanistic understanding (Deemer et al., 2016; Saunois et al., 2020; Rosentreter et al., 2021).

So far, attempts to determine global emissions have relied largely on scaling up, using an average emission extrapolation approach [critically reviewed in DelSontro et al. (2011)], or modelling using morphometric characteristics such as reservoir depth or surface area. These characteristics have been identified by regression analysis of available emission data sets as having predictive capacity. Productivity (trophic status), as measured by chlorophyll concentration is also used as a predictor (Deemer et al., 2016). This variable represents supply of autochthonous organic carbon delivered to the sediments. Allochthonous carbon (in particulate form) is another possible source of metabolizable organic carbon which can be transformed to CH_4 within the sediments. The evidence for the involvement of allochthonous carbon in CH_4 emission in reservoirs is presently limited and involves only a limited number of systems. It shows, however, that high rates of ebullition lead to high total areal fluxes of CH_4 (Aben et al., 2017), and that high C burial rates are associated with high rates of ebullition (Sobek, et al., 2012).

Ebullition of CH_4 has been observed to be the dominant flux pathway in many reservoirs (Beaulieu et al., 2020). As the source of ebullitive emissions is the organic carbon present in the sediments, there should be a strong correlation between spatial distribution of organic C rich sediments and the ebullition rate. High CH_4 fluxes were observed in Lake Wohlen (DelSontro et al., 2010), a relatively shallow run-of-river hydroelectric reservoir receiving nutrient rich treated wastewater. The CH_4 ebullition flux was unevenly distributed longitudinally along the reservoir. The dissolved CH_4 concentration in the well-mixed water column, on the other hand, increased monotonically from the riverine input end to the dam wall. Further investigation of the sediment properties of Lake Wohlen (Sobek et al., 2012) showed that there were high sedimentation rates of particulate organic matter in the middle section of the reservoir. Sediment pore water gas saturation—a prerequisite for ebullition—was greatest in these regions.

The strongest association between the location of allochthonous inputs and elevated CH_4 ebullitive emissions comes from hydroacoustic measurements in Lake Kariba, (DelSontro et al., 2011). The bubble fluxes in deltaic region, where there were significant terrestrial inputs (though not quantified), were of order ten times those in a bay which lacked riverine inflows. Similar enhanced bubble fluxes were seen at the downstream ends of a series of shallow impoundments (forebays) in the Saar River (Maeck et al., 2013), where the sediment deposition was greater than at the upstream end of the pool where the river entered. Furthermore, there was a statistically significant exponential correlation between CH_4 ebullitive flux and the measured sediment accumulation rate. Musenze et al. (2014) observed strong spatial gradients in CH_4 concentration (and by inference CH_4 emissions) in 3 subtropical reservoirs of varying catchment characteristics, surface area and morphology. The direction of the gradients was, however, the reverse of Maeck et al., 2013), being highest at the riverine input end and lowest at the dam wall end. The upstream/downstream gradient of CH_4 concentration was attributed to the selective deposition of larger, catchment-derived organic particles at the upstream end. Similar higher upstream/lower downstream gradient in CH_4 ebullition fluxes

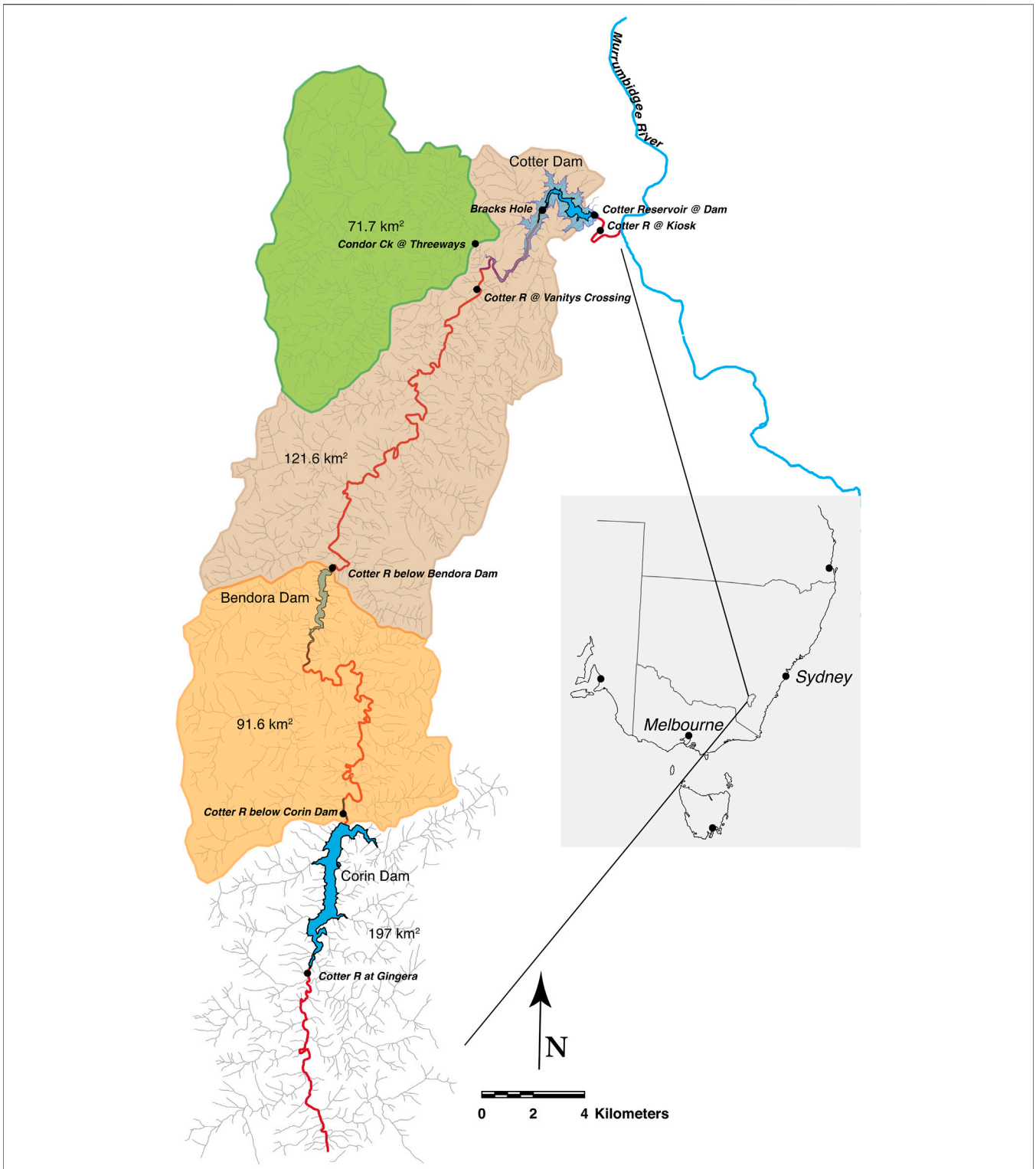

FIGURE 1 | Cotter Reservoir catchment showing hydrologic gauging stations and upstream reservoirs. Shaded areas denote catchment areas: orange between Corin and Bendora Dams; brown between Bendora and Cotter Dams not including Condor Ck; green Condor Ck subcatchment. Original full surface level of Cotter Reservoir is shown in dark blue and for enlarged Cotter Dam in light blue.

was observed in a small reservoir (McClure et al., 2020) and by the authors in two subtropical reservoirs in Australia (Sherman et al., 2012).

In all these examples the rate of input of particulate organic carbon was either constant (Lake Wohlen) or not considered. In semi-arid areas, the water and associated sediment inflows are

episodic with a single large flood event filling the reservoir. If the association of higher ebullitive CH_4 fluxes with zones of high organic sediment deposition is universally valid, then higher fluxes would be expected post flood and from the zones of greatest deposition—namely the river delta area of the reservoir (Yang, 2019). In this paper we explore this hypothesis taking advantage of fortuitous measurements on a freshwater reservoir before and after two such flood events.

2 MATERIALS AND METHODS

2.1 Site Description

Cotter Reservoir is a water supply reservoir for the city of Canberra, the capital of Australia, located at 35.320148°S, 148.939043°E, roughly 1/3 of the way between Sydney and Melbourne. At the time of the measurements, the reservoir was controlled by the original dam constructed in 1912 and enlarged to 4 GL in 1951. The full surface level (FSL) of the reservoir was 500.79 m AHD corresponding to a surface area of 47.7 ha and volume of 3.9 GL. During November 2009—October 2013, the reservoir was enlarged again to a volume of 79 GL and surface area of ca. 264 ha by construction of a new 83 m-tall dam with a full supply level of 550.8 m.

The total catchment area is 482 km^2 of which 290 km^2 comprises mid- and upper catchments supplying 2 dams, Bendora Dam and Corin Dam, located 23 and 39 river km, respectively, upstream of Cotter Dam (**Figure 1**). The mid- and upper-catchments have been protected from development within the Namadgi National Park since 1984 and vegetation there consists largely of native vegetation (e.g., eucalypt woodlands, grasslands) (Alluvium Consulting, 2020) with some limited cleared area used historically for grazing. This contrasts with most of the lower catchment immediately adjacent to Cotter Dam which has been extensively modified by forestry activities consisting of extensive pine plantations and a network of unsealed access roads. The mid- and upper-catchments comprise predominantly well-drained red Earth soils whereas the lower catchment largely consists of highly erodible yellow earths and yellow podzolics (Wade et al., 2013).

The principal gauged sources of inflow to Cotter Reservoir are Condor Creek, with a catchment of ca. 72 km^2 and in which the forestry plantations represent most of the land use; discharge from the mid- and upper-catchments that pass through Bendora Dam into the Cotter River; and discharge from the lower catchment between Bendora Dam and the gauging station at Vanitys Crossing located upstream of the confluence of the Cotter River and Condor Ck. With an area of 122 km^2 this part of the Lower Cotter catchment comprises a mixture of native vegetation within the Namadgi National Park and pine plantations. The locations of the gauging stations are shown in **Figure 1** and **Supplementary Table S1**.

2.2 Field Measurements

All floating chamber and water column profile measurements were performed from the CSIRO boat at 8–9 sites (CD01—CD09) located approximately along the axis of the reservoir (**Figure 2**). The boat was positioned at each site approximately using a handheld GPS at which point the boat was anchored and allowed to swing on the anchor line in response to changes in wind conditions. The floating chamber was tethered to the boat with a rope approximately 5 m long which allowed the chamber to move independently of the boat across the water surface (within limits); this minimized boat-induced chamber motions relative to the water surface that could potentially disturb the water beneath the chamber and potentially impact diffusive flux measurements. In practice, this means that each chamber measurement should be considered as representing the characteristic flux emanating from the area across which the chamber moved during the deployment.

2.2.1 Floating Chamber Gas Flux Measurements

Methane (and CO_2) fluxes between the water and the atmosphere were measured by recirculating air continuously at 5.5 ± 0.5 L/min through the headspace of a floating chamber and measuring this air continuously (approximately every 5 s) during a deployment of minimum duration 15-min using a Picarro G1301 $CO_2/CH_4/H_2O$ gas analyzer. The system is based on that used by Hydro Québec (Lambert and Fréchette, 2005) but with several modifications to improve performance including the implementation of the Picarro CRDS rather than using other gas analyzer technology. Technical details regarding the system are given in Zhao et al. (2015).

A minimum of two repeat deployments were performed at each site during each field trip. At sites with ebullition, deployments sometimes had to be truncated because the CH_4 concentration exceeded the measurement capabilities of the Picarro G1301: either the maximum detection limit was exceeded, or the rate of change of concentration was such that the instrument would not record values at a satisfactory rate. In such cases, additional deployments were undertaken at a site to ensure a minimum of 30 min of useable data had been acquired.

Each deployment was manually inspected for evidence of bubble evasion into the chamber—this was clearly seen as rapid substantial increases in CH_4 concentration in the headspace gas (**Supplementary Figure S1**) without corresponding changes in CO_2 concentrations. Where the data showed only a diffusive flux of CH_4, the flux was computed using a linear best fit regression to the data to yield dCH_4/dt. When ebullition was evident, end point concentrations were taken as the concentrations measured at least 15 min apart and the flux calculated as $(M_f—M_0)/\Delta t$ where M_f and M_0 are the final and initial masses of CH_4 in the chamber measured Δt seconds apart. If a deployment had been truncated due to ebullition (necessitating additional deployments as described above), a conservative estimate of the minimum total flux was determined using the end point concentrations and assuming $\Delta t = 900$ s (rather than the shorter actual measurement duration), i.e., we assumed no further emission occurred following the last usable data point. The ebullitive contribution to the total flux was calculated as the total flux less the estimated diffusive flux based on extrapolation of the diffusive portion of the deployment data.

All gas flux measurements were accompanied by meteorological data measured concurrently on the boat using

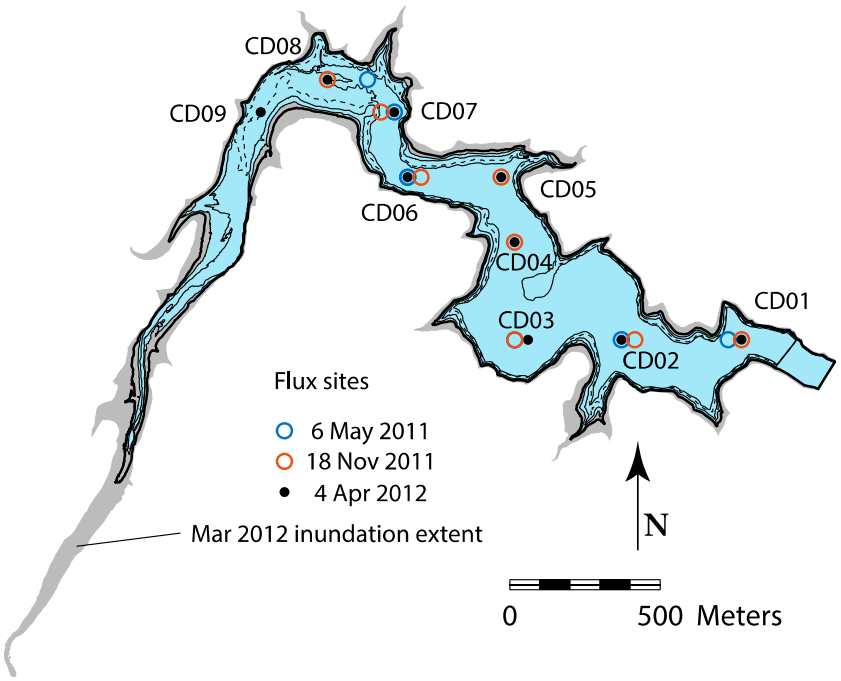

FIGURE 2 | Cotter dam GHG flux measurement sites on 6 May 2011, 18 November 2011, 4 April 2012. Maximum extents of inundation are shown as blue shaded area (504 m contour) for December 2010 and gray shaded area (512 m contour) for March 2012. Dashed line is 500 m; other contours are at 498, 502, 506 (bold) m.

a Kestrel 4500 Pocket Weather meter (barometric pressure, air temperature, relative humidity, wind speed and direction). The Kestrel 4500 was deployed on a tripod with the axis of the wind sensor approximately 0.9–0.98 m above the water surface and logged every 20 s.

Areal mean fluxes, $\bar{F}$, for each field trip were computed by weighting the flux measured at each site by the proportional contribution of the surface area of the reservoir in proximity to each site to the total reservoir surface area on the day of measurement. The boundaries between areas were defined as the approximate midpoint between measurement sites.

$$\bar{F} = \frac{\sum_i A_i F_i}{\sum_i A_i}$$

where F_i is the flux of a gas measured at site i and A_i is the corresponding subarea of the reservoir.

2.2.2 Dissolved Gas Measurements

The spatial and temporal distribution of dissolved methane was measured by collecting water samples for laboratory analysis. During flux chamber deployments, triplicate samples per measurement site were taken from a depth of 5–10 cm below the water surface during the interval between chamber deployments. Depth profiles of dissolved methane were measured by collecting triplicate samples at 2–5 depths spanning the water column at sites CD02, CD04, CD06 and CD08. Sample depths were contingent upon the water column depth at each site and were selected to ensure samples were collected near the air-water interface (0.05 m) and near the sediment-water interface (~0.5 m above the bottom). Additional samples within the water column were chosen to resolve potential gradients in dissolved methane based on inspection of water column temperature and dissolved oxygen profiles. For profiles with obvious underflows (identified by a decrease in temperature and increase in dissolved oxygen), the bottom samples were taken approximately 0.5 m above the upper boundary of the underflow. Samples were pumped from depth using a Rule bilge pump and garden hose for sufficient time to purge the hose and then the stream of water was sampled using a thrice-rinsed syringe. All water samples were stored in 12.4 mL Exetainers filled with 6.5–7.5 mL of sample plus 0.5 mL of $ZnCl_2$ preservative, leaving a headspace of 4.9–5.9 mL. All samples were sent to the Monash University Water Studies Centre for analysis of CH_4 concentration using gas chromatography. No dissolved methane samples were collected during the 6 May 2011 field trip.

2.2.3 Water Column Physical Profiles

A Yellow Springs Instruments (YSI) 6600v2 water quality sonde measured temperature, dissolved oxygen, conductivity, pH, chlorophyll-a fluorescence, phycocyanin fluorescence and turbidity. The profiler was lowered in approximately 1 m intervals and held stationary for approximately 30 s at each depth before being lowered to the next depth. Sensors were sampled every 1 s and the average, median, minimum, and maximum values for each depth computed as well as the standard deviation and variance.

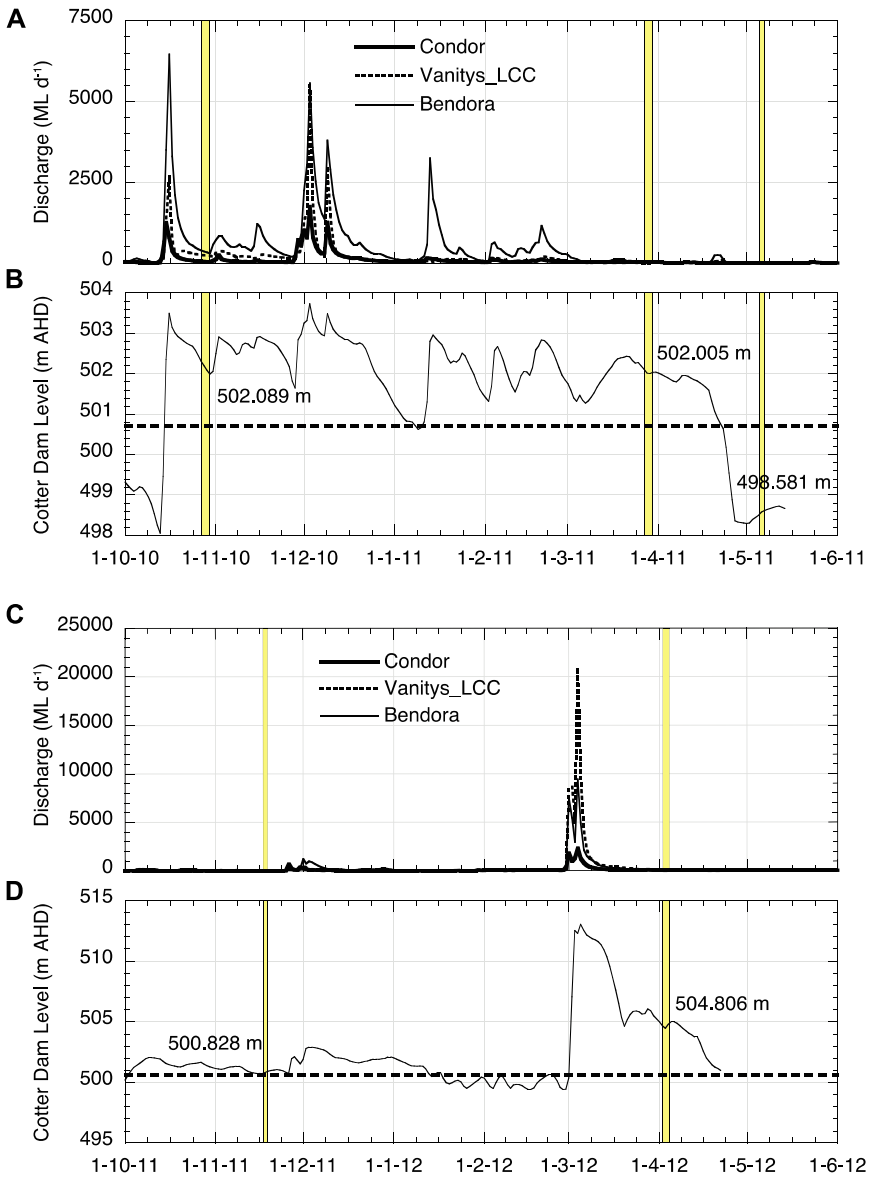

FIGURE 3 | Cotter Dam daily inflows and reservoir water levels during **(A,B)** 2010–2011; and **(C,D)** 2011–2012. Inflow data are for Condor Ck (bold), Lower Cotter Catchment at Vanitys Crossing (thin dashed line), and Cotter River below Bendora Dam (thin solid line). Discharge from the Lower Cotter Catchment was calculated as the gauged flow at Vanitys Crossing less the discharge from Bendora Dam. Heavy dashed line denotes crest of old dam. Yellow bars denote field trips and the corresponding water levels are shown as m AHD. Source data courtesy Dylan Evans, ALS, and Bureau of Meteorology << http://www.bom.gov.au/waterdata/>>.

Dissolved oxygen data within a layer were trimmed to eliminate transients associated with the relatively slow response time of the dissolved oxygen sensor.

2.3 Hydrologic Data

Hydrologic data (discharge, temperature, conductivity, and turbidity) were routinely measured every 15 min at several sites (station ID in parentheses) within the local catchment area of Cotter Reservoir: Condor Ck (410733); Cotter R. downstream of Bendora Dam (410747); Bracks Ck (340013); Cotter R. at Vanitys Crossing (410725); and downstream of Cotter Dam (410700). The water level in Cotter Dam (410704) was also recorded every 15 min. Locations of the sites are shown in **Figure 1** and **Supplementary Table S1**.

3 RESULTS

3.1 Hydrologic Conditions

Reservoir inflow and water levels are shown in **Figure 3**. The period of the study experienced the highest annual runoff in 26 years and followed the three driest years on record (2007–2009, data not shown). The flood events during

TABLE 1 | Areal mean (±s.d.) and annual methane fluxes from Cotter Reservoir and the fractional contribution of ebullition to the total flux.

Date	Reservoir surface area	Mean Areal CH_4 flux	Annual CH_4 flux	Fraction as ebullition
	[Ha]	[mg-CH_4 m^{-2} d^{-1}]	[t-CH_4 y^{-1}]	[%]
29 October 2010	54.6	4.25 (2.18)	0.86	33
29 March 2011	54.2	99.1 (21.8)	20	78
6 May 2011	39.6	9.20 (2.32)	1.9	86
18 November 2011	48.4	29.8 (12.0)	6.0	50
4 April 2012	67.0	31.6 (12.1)	6.4	74

October 2010 and December 2010 discharged 114 GL into the reservoir. This compares with a very similar amount of 118 GL from the March 2012 flood. The 2010 inflows, which raised the water level several metres above the top of the old dam (RL 500.79 m), originated approximately 15% from the Condor Ck, 25% from the Lower Cotter catchment at Vanitys Ck with the remaining 60% originating in the catchment upstream of Bendora Dam (**Supplementary Figure S2**). In contrast to the 2010 floods, the March 2012 flood originated 10% from Condor Ck, 57% from the Lower Cotter catchment at Vanitys Ck, and the remaining 34% from the upper catchment. The March 2012 flood caused the water level to rise approximately 2 m over the top of the partially-constructed new dam (RL 511.3 m) inundating soil and vegetation for the first time (**Supplementary Figure S3**). Importantly, the new dam had increased the nominal volume, and residence time, of the reservoir by a factor of ~3 compared to the previous year.

The temperature of the inflow has a profound effect on how the inflow enters the water column of the reservoir. Inflow temperature data were available for the full duration of the project at Condor Ck but only for the 2011–2012 measurement season at Vanitys Crossing. During the 2010–2011 measurement season, the water temperature in Condor Ck was 10–12°C during the October 2010 event, 15 ± 1°C from early November 2010 through mid-December 2010, and during the smaller inflow events in January 2011 the temperature varied in the range 17–20°C. During 2011–2012, there was a single large event during March 2012 at which time the temperature in Condor Ck was 14–15°C and the Cotter R at Vanitys was 1°C warmer.

From December 2011—May 2012 the temperature of the Cotter River at Vanitys Crossing was consistently 1–2°C warmer than the water in Condor Ck (**Supplementary Figure S4**). This pattern reflects the influence of the less-steep terrain and sparser vegetation cover in the Condor Ck subcatchment which allow relatively more nighttime cooling in Condor Ck. A similar pattern is expected to hold during the 2010–2011 season as well.

3.2 Gas Flux Measurements

Floating chamber measurements of CH_4 fluxes were performed at most stations during each of the five field trips. Westerly winds blowing along the axis of the water surface towards the dam prevailed during the first four trips (October 2010–November 2011, **Supplementary Figure S5**) and from the south and west during the final trip (April 2012). Wind speed during individual measurements varied from 0.2 to 3.0 m s^{-1} and averaged 1.2, 1.4, 0.8, 2.1 and 0.9 m s^{-1} for each field trip, respectively. Such conditions would produce a persistent surface drift current towards the dam that supplemented the water motions in the dam driven by inflows and outflows. Areal mean CH_4 fluxes for each trip are given in **Table 1**.

3.2.1 CH_4 Fluxes

The average and standard deviation of all CH_4 flux measurements are shown in **Figure 4** and the corresponding surface layer dissolved methane concentrations in **Figure 5**. Vertical profiles of dissolved methane at sites CD02, 04, 06, and 08 are shown in **Figure 6**. During the first field trip (October 2010), measured fluxes were low and there was only a slight spatial gradient between sites CD01 and CD07 with fluxes increasing in the upstream direction in the range 0.1–0.2 mmol CH_4 m^{-2} d^{-1}. Dissolved CH_4 varied from 0.10–0.15 μmol L^{-1} at these sites with little appreciable longitudinal variability. Ebullition was encountered only once during a single chamber deployment at site CD08 (where dissolved CH_4 was 0.18 μmol L^{-1}) and this increased the flux markedly to 0.7 mmol CH_4 m^{-2} d^{-1}. This was the only bubble event captured during the October 2010 trip despite some visual evidence of bubble activity in the vicinity of CD07 and CD08. There was no evidence of ebullition upstream of CD08.

The CH_4 fluxes measured during trip 2 (29 March 2011, mid-autumn) had increased markedly everywhere with a much more pronounced spatial gradient; the highest flux at site CD07 (32.3 ± 5.2 mmol m^{-2} d^{-1}) was more than 100 times the lowest flux at site CD01 (0.28 ± 0.019 mmol m^{-2} d^{-1}). Bubbles were conspicuous at all times at sites CD06 - CD08 and were occasionally seen at CD05 and CD03. Only four chamber deployments did not record a bubble event and site CD01 was the only site without any bubble event reported. Similarly, dissolved CH_4 exhibited a very pronounced longitudinal gradient, increasing from 0.31 μmol L^{-1} at CD01 to >2.6 μmol L^{-1} at sites CD07 and CD08.

By late autumn (6 May 2011), after significant seasonal cooling of the water column had taken place (**Figure 7**), the fluxes had diminished at all sites. Fluxes measured at sites CD01 to CD06 were the lowest during the project but the 100:1 gradient of fluxes from upstream to downstream persisted. Bubble activity in May 2011 was pronounced at both sites CD07 and CD08, but absent from all other sites.

The following late spring trip (November 2011) found higher fluxes everywhere compared to May 2011, but the strength of the longitudinal gradient had diminished to approximately 10:1 and the strength of the corresponding gradient in dissolved CH_4 had also diminished. Again, ebullition was present at just the upstream sites

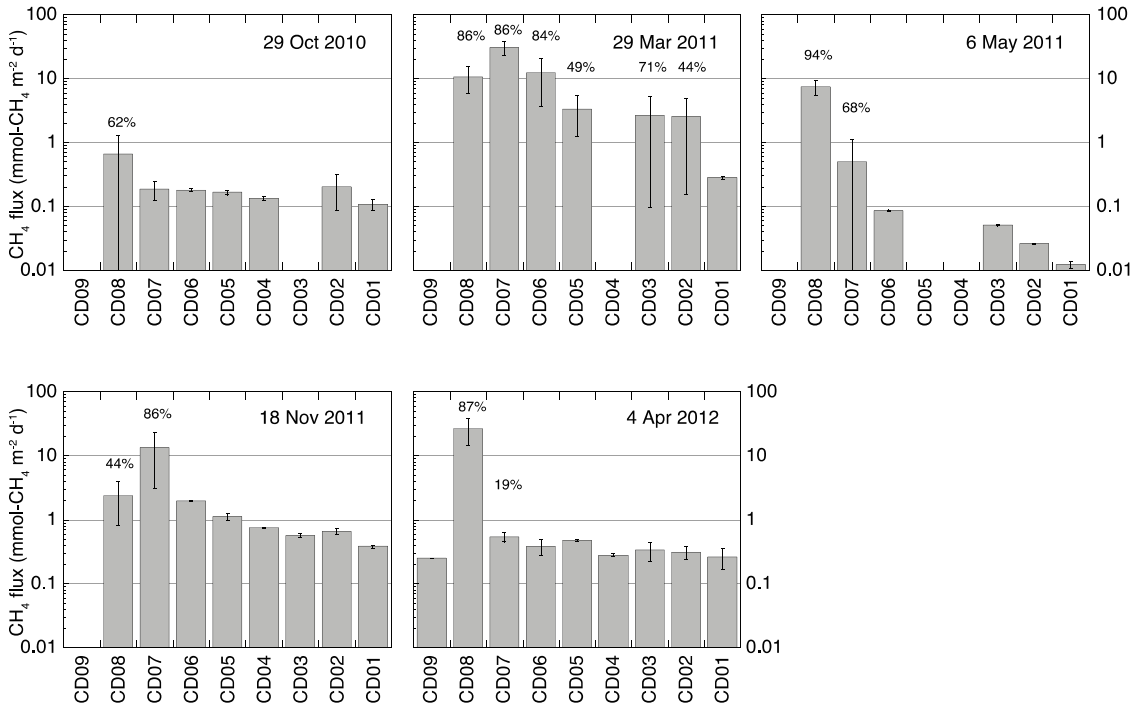

FIGURE 4 | Average 15-min methane fluxes (mmol-CH_4 m^{-2} d^{-1}) measured at each site during the five field trips: 29 October 2010. 29 March 2011, 6 May 2011, 18 November 2011, 4 April 2012. Missing bars indicate no measurement performed. Percentages above bars are the fraction of the measured fluxes attributable to ebullition. Error bars denote one sample standard deviation.

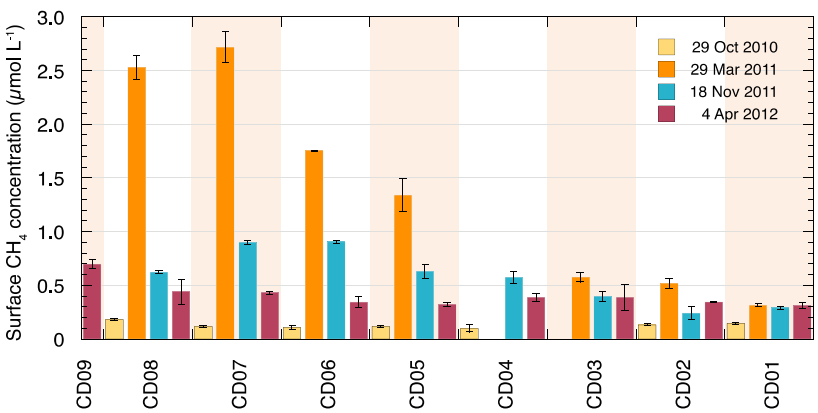

FIGURE 5 | Dissolved methane concentration just below the water surface during the flux chamber measurements on 29 October 2010 (beige), 29 March 2011 (orange), 18 November 2011 (blue) and 4 April 2012 (violet). Note that site CD04 was not measured in March 2011 and CD03 was not measured in October 2010. Site CD09 is upstream, site CD01 is downstream.

CD07 and CD08. Ebullition was the dominant mode of emission at CD07.

By the following autumn (April 2012), the gradient in fluxes had returned to close to the level originally observed in October 2010 (neglecting site CD08). Ebullition was the dominant (87%) component of the total CH4 flux at CD08. The gradient in dissolved CH_4 also weakened by a further factor of 2 compared to that observed in November 2011. Notably, both fluxes and dissolved CH_4 were consistently higher in April 2012 compared to October 2010 and this may relate to the difference in water temperatures at the times of the two field trips (discussed below).

In November 2011, ebullition was most intense at site CD07 whereas during April 2012 bubble activity was mainly at CD08. In April 2012, significant bubble activity was observed over extensive areas in the vicinity of site CD09, a newly inundated

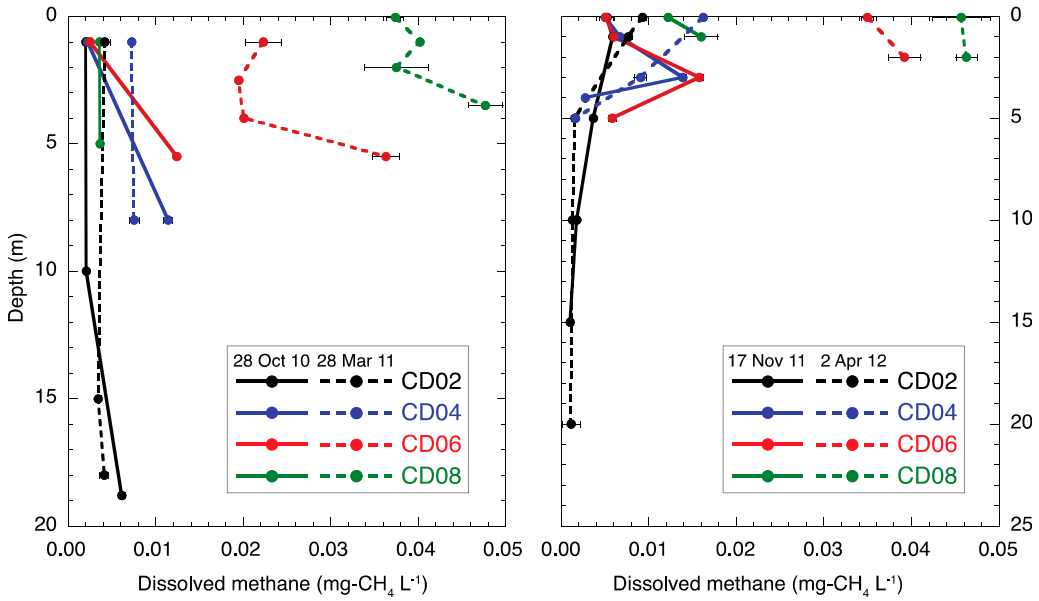

FIGURE 6 | Depth profiles of dissolved CH_4 on 28 October 2010 (solid), 28 March 2011 (dashed), 17 November 2011 (solid), and 2 April 2012 (dashed) at sites CD02 (black), CD04 (blue), CD06 (red) and CD08 (green). Error bars denote 1 standard deviation (n = 2).

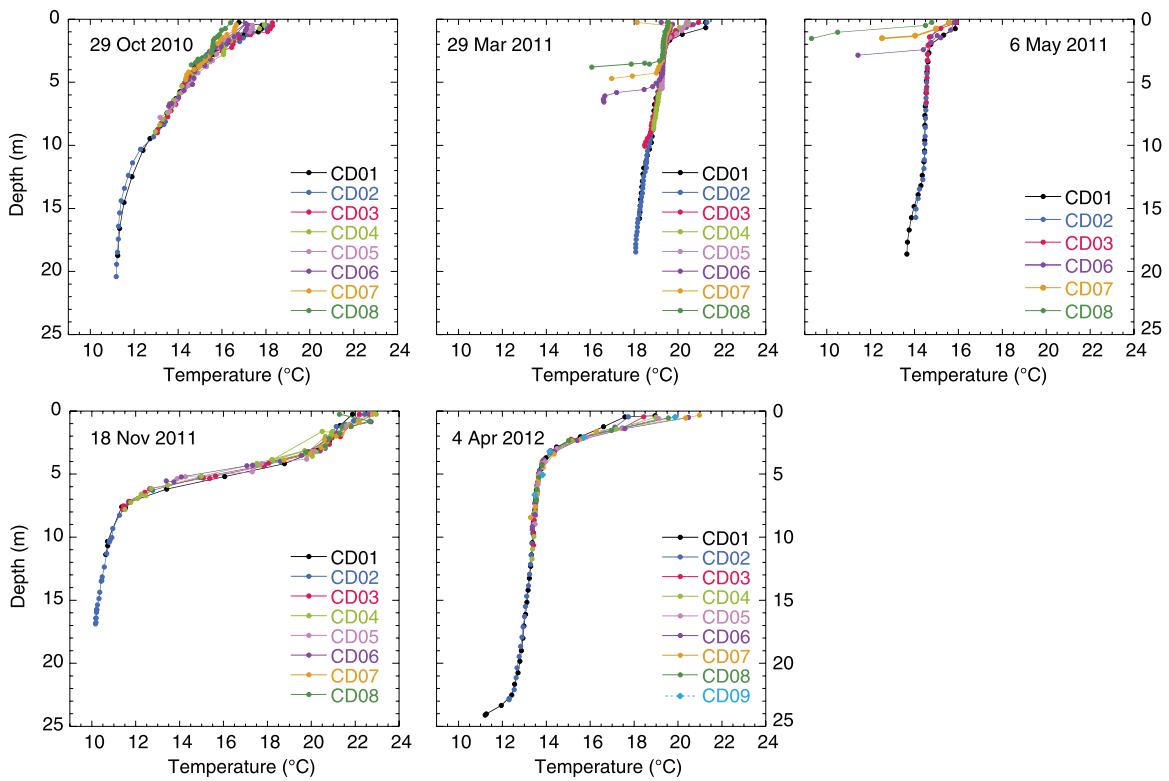

FIGURE 7 | Water column temperature profiles at each site during the five field trips: 29 October 2010. 29 March 2011, 6 May 2011, 18 November 2011, 4 April 2012.

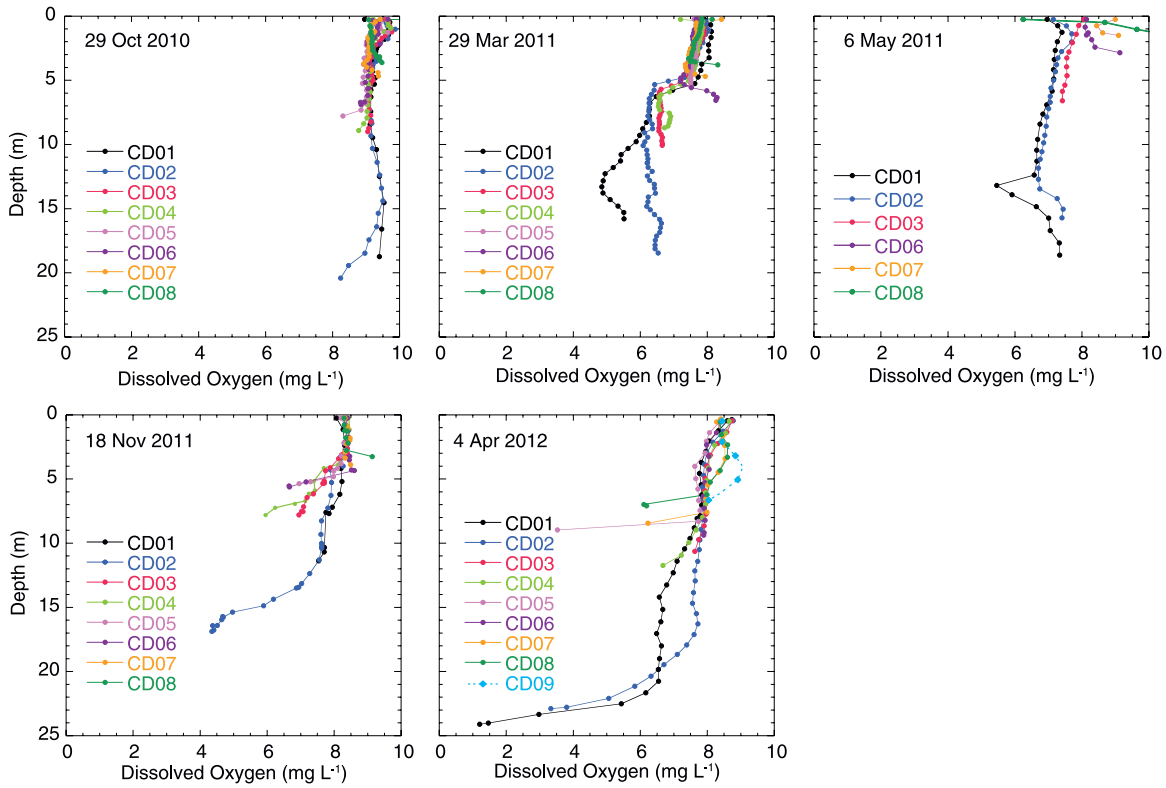

FIGURE 8 | Water column dissolved oxygen profiles at each site during the five field trips: 29 October 2010. 29 March 2011, 6 May 2011, 18 November 2011, 4 April 2012.

and possible deposition zone, but was not detected in the flux chamber measurements.

3.2.2 Areal Mean CH_4 fluxes

Averaged over the surface of the reservoir, the areal mean CH_4 flux increased by a factor of 23 from 4.25 mg-CH_4 m^{-2} d^{-1} in October 2010 to 99.1 mg-CH_4 m^{-2} d^{-1} in March 2011 following the first two flood events before decreasing to 9.20 mg-CH_4 m^{-2} d^{-1} in mid-autumn (**Table 1**). Mean areal CH_4 fluxes during 2011–2012 were the same (*t*-test of means, $p = 0.95$) at 29.8 and 31.6 mg-CH_4 m^{-2} d^{-1} before and after the March 2012 flood.

3.3 Reservoir Stratification

Temperature profile data (**Figure 7**) show that inflow events caused extensive mixing throughout the water column of the reservoir. The 29 October 2010 profile shows a hypolimnion temperature of 11°C—about 1°C warmer than similar observations in preceding years (unpublished data)—but with evidence of extensive disturbance and mixing of the water column over the top 10 m. By 29 March 2011, the hypolimnion temperature had increased to 18°C and the temperature gradient was linear from top-to-bottom, a condition that can only be caused by significant whole-water column mixing which presumably was the result of the December 2010 flood and the follow-up runoff event in January 2011. Autumnal cooling of the water column typically begins in April in this region and by 6 May 2011 seasonal cooling had caused full mixing throughout the water column which had cooled to 14°C at the bottom.

During 2011–2012, the water column exhibited a "typical" late spring temperature profile on 18 November 2011 with a hypolimnion temperature of 10°C and a very strong thermocline from 3 to 8 m depth. Following the March 2012 flood event, the 4 April 2012 profile shows that, despite the very large volume of inflow arriving at the dam in March (>120,000 mL), there was only limited warming of the hypolimnion to 11–13°C. The lack of greater hypolimnetic warming compared to the December 2010—January 2011 flood events was likely a consequence of the relatively warm inflow temperature (14–16°C) that would constrain the inflow to enter the reservoir, after entrainment of surface layer water, to the uppermost 5–10 m. The temperature at the sediment-water interface did not exceed ca. 13°C during the 2011–2012 season.

The strong difference between thermal stratification characteristics between years, with 2010–2011 at least 5°C warmer than 2011–2012, could be expected to have a substantial impact on any thermally regulated microbial processes in the reservoir such as methanogenesis.

The dissolved oxygen profiles (**Figure 8**) are consistent with this description of the physical mixing processes within the water column. Water column dissolved oxygen seldom fell below 6 mg-O_2 L^{-1}, a highly unusual condition close to the sediment-water

interface in a monomictic reservoir. (Note that oxygen profiles were not measured at the deepest part of the reservoir, thus local hypoxia cannot be excluded.) Dissolved oxygen was <4 mg O_2 L^{-1} on only one occasion (4 April 2012)—at sites CD01 and CD02 when the reservoir was at its deepest during the project.

The very weak vertical gradients in dissolved oxygen during 2010–2011suggest a combination of relatively high rates of vertical mixing and/or very low *in situ* oxygen demand in the hypolimnion. Given the elevated temperatures at depth during this season, and the recent large supply of organic matter, low oxygen demand seems less likely. Profiles from both 18 November 2011 and 4 April 2012 trips showed stronger gradients in dissolved oxygen close to the bottom of the water column indicating that sediment oxygen demand exceeded the turbulent diffusive supply of oxygen from above to a greater extent in 2011–12 compared to 2010–11.

Thermal stratification exhibited little longitudinal variability at depth with only minor divergences from one end of the reservoir to the other during each field trip apart from the measurements on 29 March 2011 and 6 May 2011 (**Figure 7**). At stations CD06, CD07, and CD08 a cold underflow is apparent in the lowest 2 m of each profile. This underflow was characterised also by relatively elevated dissolved oxygen concentrations (**Figure 8**). During the week prior to 29 March 2011, steady inflow to Cotter Reservoir from Bendora Dam averaged 0.6 m^3 s^{-1} and 0.4 m^3 s^{-1} from Condor Ck with temperatures in both streams steadily decreasing from 17 to 14°C. Just prior to 6 May, total inflow was 0.6 m^3 s^{-1} and a cold change in weather had decreased the stream temperature to 7–9°C, again consistent with the temperature of the underflow in the upper reaches of the reservoir and the development of a relatively colder lower 5 m of the water column further downstream. We note also that the seasonality and the observed temperature and dissolved oxygen differences are both tell-tale indicators of differential cooling (Wells and Sherman, 2001; Doda et al., 2022).

The biogeochemical consequences are that water from the upstream end of the reservoir, which is enriched in methane relative to the downstream stations (**Figure 6**), is translocated by a density current to deeper waters downstream. The overlying waters are effectively displaced upwards forming a methane-depleted surface layer flowing upstream towards the littoral area. This temperature differential was not seen during the final field trip (4 April 2012) when the seasonality was theoretically appropriate, but the weather was 3–5°C warmer than the prior year. Also, at this time the reservoir was 5 m deeper and the littoral zone—the source of the cooler and methane-enriched water had moved further upstream beyond station CD9 and was not detected by the sampling at this station.

Especially noteworthy is that the water column at the upstream littoral sites where the highest CH_4 fluxes were measured was always well oxygenated at the deepest point in the profile. This is consistent with the CH_4 production occurring in the sediments at these sites. The gravity currents moving methane enriched water downstream as a subsurface flow will transfer oxygenated littoral waters to the deeper reaches downstream also.

4 DISCUSSION

The profound hydrologic events caused by drought breaking rains in the catchment were followed by a substantial increase in methane emissions across the entire reservoir. As we show below, part of this increase is due to the observed changes in the stratification and sediment temperature produced by the inflows. A larger part of the increased emissions is attributed to the delivery of large amounts of allochthonous particulate organic carbon by the flood pulses.

4.1 Temperature and Stratification Effects

The impact of the large inflow volumes in late spring—early summer of 2010 on the relatively small reservoir was to completely mix the water column (**Figure 7**). In addition to the two large floods, inflow averaged >550 mL d^{-1} from September 2010 through February 2011. The nearly linear temperature stratification—as opposed to the more typical stratification of progressively increasing dT/dz as one approaches the bottom of the surface mixing layer from below—seen in other years (data not shown) in this monomictic reservoir confirms that profound mixing occurred. This mixing effect raised the bottom temperature from its typical seasonal value of ca. 10–18°C throughout the length of the reservoir.

The evidence indicates that the combined impact of the large inflow events on temperature stratification and the increased deposition of catchment organic matter was responsible for the 23-fold increase, relative to the first measurement on 29 October 2010, in reservoir CH_4 emissions observed following the first runoff event in late 2010 and the 7-fold increase observed the following year. It is significant that during the second year of the study, the large inflow event occurred in early autumn (March 2012) rather than late spring (mid-October 2010) because thermal stratification in the reservoir was stronger—the top to bottom temperature difference was 10–12°C for the second event compared to just 6°C for the first event. The stronger stratification and deeper water column appear to have prevented mixing all the way to the bottom of the water column in 2012 although there was sufficient mixing energy to create a linear temperature gradient. During 2012, the hypolimnion temperature was just 13°C compared to 18°C during the previous year.

Seasonal temperature differences alone cannot explain the variability in CH_4 emissions, as emissions were higher in November 2011 than in April 2012 despite the water column being cooler in November. The higher average wind speed (**Supplementary Figure S5**) during the November 2011 measurements would be expected to enhance the diffusive flux and partially compensate for a decrease in methane production rate due to the colder water temperatures. As well, ebullition may have been additionally suppressed by the 4 m deeper water column in April.

Assuming measurements of thermal mediation of methane production by other researchers (Duc et al., 2010; Lofton et al., 2014) are applicable to Cotter Reservoir, we suggest that temperature effects alone increased methane emissions by 2–7 times following the 2010–2011 floods and by 1.3–2 times following the March 2012 flood. If we assume the higher estimates for each year, then the increased supply of catchment organic matter accounted for an additional increase in emissions by a factor of 3.3–3.5 during both years.

4.2 Delivery of Allochthonous Organic Carbon

The supply of catchment organic matter has been hypothesized to be responsible for consistent spatial patterns of CH_4 emissions by the authors in other storages in Australia (Sherman et al., 2012) and elsewhere (**Section 1**). The 2010 inflow was, we suggest, an event which delivered unusually large amounts of reactive organic matter to the reservoir.

The late 2010 inflow event was the first significant inflow event since the onset of the Millennium Drought of 2002–2009 in eastern Australia. Much of the catchment vegetation was *Eucalyptus* spp. which shed their leaves annually and, under conditions of extreme drought die off, adding further to the accumulated leaf litter. Under drought conditions there would have been an unusually large build up of organic matter. In addition, the lower catchment was only slowly recovering from the effects of the devastating 2003 Canberra bushfire. Landscape recovery activities undertaken prior to the floods had left substantial piles of debris in a highly disturbed, erosion-prone Lower Cotter subcatchment (Wade et al., 2013). It is reasonable to expect that the drought-breaking runoff transported a particularly large amount of eroded soil and terrestrial organic matter which had been accumulating in the catchment over the preceding years. This sediment and organic matter would be deposited in the reservoir with much of it focused in the upstream reaches of the water body as the inflow decelerated and heavier particulates fell out to the bottom. Such an increase of organic matter towards the upstream end of the reservoir is consistent with our observations of increasing CH_4 fluxes as the upstream end of the reservoir was approached (**Figure 4**).

The impact of the 2003 Canberra bushfire—which devasted the Cotter catchment—should be considered as well. In addition to the relatively high hillside and gully erosion potential of the landscape arising from historical forestry operations close to the reservoir, the bushfire destroyed most of the vegetation in this area and burned hot enough to change the soil properties in a way that would further exacerbate erosion. Post-fire activities in the nearby catchment included large scale harvesting of salvageable timber (Wade et al., 2013) with the consequence that at the time of our measurements most of the immediate catchment consisted mainly of grasses and scrubby vegetation (e.g., blackberries) and occasional log piles. We assume that both the bushfire itself and the post-fire management activities further increased the susceptibility of the catchment to erosion and added to the supply of readily eroded or transported organic matter.

4.3 Increased CH_4 Fluxes and Increased Ebullition Post Deposition Events

Even after allowing for the different temperature effects after the 2 flood events, average methane emissions were up to 3.5 times greater than before the floods. These effects are most clearly seen at Site CD08 where the CH_4 flux is the largest of all sites post flood and increased by a factor of about 100. This increase represents the transition from a flux characteristic of an "old" reservoir (4.3 mg-CH_4 m^{-2} d^{-1}) to the much higher and ebullition-dominated fluxes (99 mg-CH_4 m^{-2} d^{-1}) similar to those of the allochthonous influenced sites in the lake Wohlen (DelSontro et al., 2010) and Saar River impoundments (Maeck et al., 2013) (discussed in Section1).

Emissions at site CD08 had been the only ebullition emissions before the flood whereas ebullition occurred at six of the seven sites measured following the first flood. At 4 of these post-flood sites, ebullition was the dominant contributor (relative to diffusion) to the total flux (**Figure 4**). The effect of the floods was to extend the higher flux and ebullition-rich zone further into the dam towards the dam wall.

The behavior of CD08 is noteworthy in that ebullition was the larger component of the total CH_4 flux on all 5 sampling visits, even though the magnitude of the flux varied by a factor of 20 across the measurements. Furthermore, the site was always in oxygenated water (**Figure 8**). We attribute this effect to its location in the river delta section of the reservoir—the region of trapping of incoming particulate organic debris even under regular or low flow conditions—providing a continuing input of fresh reactive organic matter.

4.4 Implications

There are 2 major implications from this work: methane fluxes from "old" reservoirs (those where the original *in situ* supply of reactive organic carbon, inundated on dam construction, has been exhausted) may be stimulated by episodic events. This increase is a step change in the total CH_4 flux and persists for some time. These episodic events deliver uneven distributions of new, reactive allochthonous carbon to the reservoir which support higher rates of CH_4 emission reflecting the sedimentation pattern of the new material within the reservoir. The distribution of sediment within the reservoir is dependent on the residence time of the flood pulse within the reservoir, the inflow sediment concentration, and the sedimentation rate of the material in the pulse. Consequently, the location of sediment zones (and high emission areas) may vary from event to event and change location and extent within the reservoir depending on the source and size of the flood.

Much of the existing data on reservoir CH_4 emissions are based on studies with limited temporal coverage, i.e., based on time-limited field measurement campaigns that cannot realistically be expected to incorporate interannual to decadal hydrographic perturbations.

Our results suggest that major episodic hydrological disturbances can have a large impact on measured reservoir CH_4 emissions and that these effects persist for at least a year. The timing of field measurements relative to hydrological events should be considered when extrapolating from brief periods of field observations to decadal and longer

estimates of reservoir emissions used in Greenhouse Inventory accounting.

Furthermore, better understanding of catchment properties, especially the reactivity and quantities of mobilizable particulate organic carbon, is necessary for predicting reservoir emissions in the face of climate change.

DATA AVAILABILITY STATEMENT

The raw data supporting the conclusion of this article will be made available by the authors, without undue reservation.

AUTHOR CONTRIBUTIONS

BSS and PWF developed the experimental design and performed all the sampling and data analysis. BSS wrote the preliminary report with assistance from PWF including preparation of all figures. Both authors wrote the main manuscript text, interpreted the data, discussed the results, and reviewed the manuscript.

FUNDING

Financial support for the "Cotter Dam Methane Emissions" project was provided by Icon Water (formerly ACTEW) and CSIRO's Integrated Water Systems stream in the Urban Water theme. Financial support for publication was provided by the University of Canberra Centre for Applied Water Science and Reservoir Doctors Pty Ltd.

ACKNOWLEDGMENTS

The authors would like to thank Icon Water and Marco Bottari (Icon Water) for permission and support to conduct this work at Cotter Reservoir; Jim Brophy (CSIRO) and Danny Hunt (CSIRO) for their valuable technical support in carrying out the field work; and to Drs. Todd Scicluna and Perran Cook (Monash University Water Studies Centre) for performing the gas chromatography. Special thanks to Dr. Jon Sanderman for valuable comments on the project reports which formed the basis of this manuscript. We also wish to thank two reviewers for their very helpful and insightful comments which have led to a substantially improved manuscript.

SUPPLEMENTARY MATERIAL

The Supplementary Material for this article can be found online at: https://www.frontiersin.org/articles/10.3389/fenvs.2022.893180/full#supplementary-material

REFERENCES

Aben, R. C. H., Barros, N., van Donk, E., Frenken, T., Hilt, S., Kazanjian, G., et al. (2017). Cross Continental Increase in Methane Ebullition under Climate Change. *Nat. Commun.* 8, 1682. doi:10.1038/s41467-017-01535-y

Alluvium Consulting (2020). *Cotter Catchment Actions for Clean Water Plan*. Canberra: Alluvium Consulting.

Beaulieu, J. J., Waldo, S., Balz, D. A., Barnett, W., Hall, A., Platz, M. C., et al. (2020). Methane and Carbon Dioxide Emissions from Reservoirs: Controls and Upscaling. *J. Geophys Res. Biogeosci* 125, e2019JG005474. doi:10.1029/2019JG005474

Deemer, B. R., Harrison, J. A., Li, S., Beaulieu, J. J., DelSontro, T., Barros, N., et al. (2016). Greenhouse Gas Emissions from Reservoir Water Surfaces: A New Global Synthesis. *BioScience* 66, 949–964. doi:10.1093/biosci/biw117

Deemer, B. R., and Holgerson, M. A. (2021). Drivers of Methane Flux Differ between Lakes and Reservoirs, Complicating Global Upscaling Efforts. *Biogeosciences* 126, e2019JG005600. doi:10.1029/2019jg005600

DelSontro, T., Kunz, M. J., Kempter, T., Wüest, A., Wehrli, B., and Senn, D. B. (2011). Spatial Heterogeneity of Methane Ebullition in a Large Tropical Reservoir. *Environ. Sci. Technol.* 45, 9866–9873. doi:10.1021/es2005545

DelSontro, T., McGinnis, D. F., Sobek, S., Ostrovsky, I., and Wehrli, B. (2010). Extreme Methane Emissions from a Swiss Hydropower Reservoir: Contribution from Bubbling Sediments. *Environ. Sci. Technol.* 44, 2419–2425. doi:10.1021/es9031369

Doda, T., Ramón, C. L., Ulloa, H. N., Wüest, A., and Bouffard, D. (2022). Seasonality of Density Currents Induced by Differential Cooling. *Hydrol. Earth Syst. Sci.* 26, 331–353. doi:10.5194/hess-26-331-2022

Duc, N. T., Crill, P., and Bastviken, D. (2010). Implications of Temperature and Sediment Characteristics on Methane Formation and Oxidation in Lake Sediments. *Biogeochemistry* 100, 185–196. doi:10.1007/s10533-010-9415-8

Etiope, G., and Schwietzke, S. (2019). Global Geological Methane Emissions: An Update of Top-Down and Bottom-Up Estimates. *Elem. Sci. Anthropocene* 7, 47. doi:10.1525/elementa.383

Lambert, M., and Fréchette, J.-L. (2005). "Analytical Techniques for Measuring Fluxes of CO2 and CH4 from Hydroelectric Reservoirs and Natural Water Bodies," in *Greenhouse Gas Emissions - Fluxes and Processes: Hydroelectric Reservoirs and Natural Environments*. Editors A. Tremblay, L. Varfalvy, C. Roehm, and M. Garneau (Berlin, Heidelberg: Springer Berlin Heidelberg), 37–60. doi:10.1007/978-3-540-26643-3_3

Lan, X., Basu, S., Schwietzke, S., Bruhwiler, L. M. P., Dlugokencky, E. J., Michel, S. E., et al. (2021). Improved Constraints on Global Methane Emissions and Sinks Using δ13C-CH4. *Glob. Biogeochem. Cycles* 35, e2021GB007000. doi:10.1029/2021gb007000

Lofton, D. D., Whalen, S. C., and Hershey, A. E. (2014). Effect of Temperature on Methane Dynamics and Evaluation of Methane Oxidation Kinetics in Shallow Arctic Alaskan Lakes. *Hydrobiologia* 721, 209–222. doi:10.1007/s10750-013-1663-x

Lynch, J., Cain, M., Pierrehumbert, R., and Allen, M. (2020). Demonstrating GWP*: A Means of Reporting Warming-Equivalent Emissions that Captures the Contrasting Impacts of Short- and Long-Lived Climate Pollutants. *Environ. Res. Lett.* 15, 044023. doi:10.1088/1748-9326/ab6d7e

Maeck, A., DelSontro, T., McGinnis, D. F., Fischer, H., Flury, S., Schmidt, M., et al. (2013). Sediment Trapping by Dams Creates Methane Emission Hot Spots. *Environ. Sci. Technol.* 47, 8130–8137. doi:10.1021/es4003907

McClure, R. P., Lofton, M. E., Chen, S., Krueger, K. M., Little, J. C., and Carey, C. C. (2020). The Magnitude and Drivers of Methane Ebullition and Diffusion Vary on a Longitudinal Gradient in a Small Freshwater Reservoir. *J. Geophys. Res. Biogeosciences* 125, e2019JG005205. doi:10.1029/2019jg005205

Musenze, R. S., Grinham, A., Werner, U., Gale, D., Sturm, K., Udy, J., et al. (2014). Assessing the Spatial and Temporal Variability of Diffusive Methane and Nitrous Oxide Emissions from Subtropical Freshwater Reservoirs. *Environ. Sci. Technol.* 48, 14499–14507. doi:10.1021/es505324h

Prather, M. J., Holmes, C. D., and Hsu, J. (2012). Reactive Greenhouse Gas Scenarios: Systematic Exploration of Uncertainties and the Role of Atmospheric Chemistry. *Geophys. Res. Lett.* 39, L09803. doi:10.1029/2012gl051440

Rosentreter, J. A., Borges, A. V., Deemer, B. R., Holgerson, M. A., Liu, S., Song, C., et al. (2021). Half of Global Methane Emissions Come from Highly Variable Aquatic Ecosystem Sources. *Nat. Geosci.* 14, 225–230. doi:10.1038/s41561-021-00715-2

Saunois, M., Stavert, A. R., Poulter, B., Bousquet, P., Canadell, J. G., Jackson, R. B., et al. (2020). The Global Methane Budget 2000–2017. *Earth Syst. Sci. Data* 12, 1561–1623. doi:10.5194/essd-12-1561-2020

Sherman, B., Ford, P., Hunt, D., and Drury, C. (2012). *Reservoir Methane Monitoring and Mitigation - Little Nerang and Hinze Dam Case Study*. Brisbane: Urban Water Security Research Alliance. Available at: https://publications.csiro.au/rpr/pub?pid=csiro:EP124042.

Shindell, D., Kuylenstierna, J. C. I., Vignati, E., van Dingenen, R., Amann, M., Klimont, Z., et al. (2012). Simultaneously Mitigating Near-Term Climate Change and Improving Human Health and Food Security. *Science* 335, 183–189. doi:10.1126/science.1210026

Sobek, S., DelSontro, T., Wongfun, N., and Wehrli, B. (2012). Extreme Organic Carbon Burial Fuels Intense Methane Bubbling in a Temperate Reservoir. *Geophys. Res. Lett.* 39, L01401. doi:10.1029/2011gl050144

Turner, A. J., Frankenberg, C., and Kort, E. A. (2019). Interpreting Contemporary Trends in Atmospheric Methane. *Proc. Natl. Acad. Sci. U.S.A.* 116, 2805–2813. doi:10.1073/pnas.1814297116

Wade, A., White, I., Worthy, M., Gill, A. M., Mueller, N., Taylor, P., et al. (2013). Land Management Impacts on Water Quality Following Fire in a Major Water Supply Catchment. *Australas. J. Water Resour.* 16, 121–139. doi:10.7158/w10-841.2013.16.2

Wells, M. G., and Sherman, B. (2001). Stratification Produced by Surface Cooling in Lakes with Significant Shallow Regions. *Limnol. Oceanogr.* 46, 1747–1759. doi:10.4319/lo.2001.46.7.1747

Yang, L. (2019). Contrasting Methane Emissions from Upstream and Downstream Rivers and Their Associated Subtropical Reservoir in Eastern China. *Sci. Rep.* 9, 8072. doi:10.1038/s41598-019-44470-2

Zhao, Y., Sherman, B., Ford, P., Demarty, M., DelSontro, T., Harby, A., et al. (2015). A Comparison of Methods for the Measurement of CO2 and CH4 Emissions from Surface Water Reservoirs: Results from an International Workshop Held at Three Gorges Dam, June 2012. *Limnol. Oceanogr. Methods* 13, 15–29. doi:10.1002/lom3.10003

Conflict of Interest: The authors declare that the research was conducted in the absence of any commercial or financial relationships that could be construed as a potential conflict of interest. At the time the project was undertaken (2010-2012), both BSS and PWF were solely employed by CSIRO. Reservoir Doctors Pty Ltd. is a sole proprietor company established in 2014 by BSS to facilitate undertaking part-time ad hoc consulting work following his departure/retirement from CSIRO in late 2013. BSS continues as a visiting scientist at CSIRO and an Adjunct Associate Professor at the Centre for Applied Water Science, University of Canberra, Bruce, ACT, Australia.

Publisher's Note: All claims expressed in this article are solely those of the authors and do not necessarily represent those of their affiliated organizations, or those of the publisher, the editors and the reviewers. Any product that may be evaluated in this article, or claim that may be made by its manufacturer, is not guaranteed or endorsed by the publisher.